Integration of Interdigitated Electrodes in Split Ring Resonator for Detecting Liquid Mixtures

Xiue Bao, *Student Member, IEEE,* Meng Zhang, Ilja Ocket, *Member, IEEE,* Juncheng Bao, Dries Kil, Zhuangzhuang Liu, Robert Puers, *Fellow, IEEE,* Dominique Schreurs, *Fellow, IEEE,* and Bart Nauwelaers, *Senior Member, IEEE*

***Abstract*—A microwave microfluidic sensor for detecting binary liquid mixtures with a dielectric method at RF/microwave frequencies is presented in this paper. The sensor is based on a split ring resonator (SRR) that is implemented in a microstrip transmission line, with interdigitated electrodes (IDE) being integrated in the ring for liquid detection. Based on the equivalent circuit of the IDE-SRR device and with a series of finite element simulations, the detection theory is developed and the device design optimization is investigated. The validation measurements on water-isopropanol liquid mixtures with various of concentrations show that the proposed IDE-SRR sensor has higher sensitivity than previous standard SRR sensor. The IDE-SRR sensor is then used to detect two binary liquids, i.e., water-methanol mixtures and water-tetrahydrofuran mixtures. The measured effective permittivity results of the binary mixtures at RF/microwave frequency range are compared to the existing mixing models for binary dielectric mixtures at zero frequency.**

***Index Terms*—Effective permittivity, interdigitated electrodes, liquid mixtures, mixing theory, split ring resonator.**

I. Introduction

DIELECTRIC spectroscopy, which measures the dielectric responses of a material to electromagnetic fields, is an important and widely used material characterization technique. The spectroscopy characterization technique has also been carried out to extract a wealth of information about the physiological properties of biological materials [1]. The popularity of this technique is due to its simple, easy to use, non-invasive, and real time nature [2]–[7]. In recent years, the integration of permittivity measurement techniques with microfluidic devices has made the technology increasingly attractive in biological and chemical applications, as it has many advantages including high sensitivity, robustness, and low fabrication cost [8]–[11].

However, the use of dielectric spectroscopy is based on the assumption that the material under observation is homogeneous and isotropic, which in the strict sense could not describe actual situation in nature. Therefore, the effective medium approximation (EMA) is proposed to describe the permittivity of mixtures, leading to various mixing models [12]–[14]. Conceptually, the mixing models assume that inclusions or constituents are evenly distributed within a homogeneous system. They have been used to analyze heterogeneous media composed of two-phase and even multi-phase constituents, including composite materials [15] and biological suspensions [16]. Nevertheless, applications of the EMA formulas mainly focus on static analysis of dielectric media. It thus might be meaningful to extend the mixing theories to radio frequencies and microwaves.

Within this context, this paper focuses on the measurement of effective permittivity of a simple mixture type - the binary liquid mixtures at RF/microwave frequencies. The measurement sensor herein used is based on a split ring resonator (SRR) excited by a microstrip transmission line, using interdigitated electrodes (IDE) [17] as sensing area. The SRR microwave sensing platform is developed using the concept of metamaterials, as the main advantages of a metamaterial resonator include its high sensitivity to a small amount of dielectric material, which is obviously promising for sensing applications [18]–[21]. Using this concept, various types of metamaterial sensors have been introduced so far for different sensing applications [20]–[22], among which the SRR sensor is a typical example. Some prominent studies of SRR sensors based on different configurations were developed, which represent the state-of-the-art. For instance, *Lee et al.* proposed some SRR-based biosensors for the detection of biotin and streptavidin binding [23] and DNA sensing [24] and *Velez et al.* developed some SRR sensors for liquid measurements [25]–[27]. However, most SRR sensors are designed as a simple gap located at the split ring, whereas in the proposed IDE-SRR sensor, a group of IDEs are integrated within the SRR to replace the traditional gap, working as the sensing area to detect dielectric liquid mixtures with high sensitivity. The interdigitated structure, which is widely used in RF/microwave electronic circuits as a capacitor, is able to provide high sensitivity to the dielectric materials under investigation [28], [29]. The IDE-SRR sensor

Manuscript received October 13, 2019; revised December 24, 2019; accepted January 20, 2020. This work was supported in part by the KU Leuven under project C24/15/015 Microwave Microbiology (μ^2BIO), in part by the KU Leuven under project Hercules, and in part by the MTT-S 2018 Graduate Fellowship. This paper is an expanded version from the IEEE MTT-S International Microwave Workshop Series on Advanced Materials and Processes 2019, July 16th-18th, 2019, Bochum, Germany. *(Corresponding author: Meng Zhang (e-mail: meng.zhang@esat.kuleuven.be).)*

X. Bao, M. Zhang, J. Bao, D. Schreurs, and B. Nauwelaers are with the TELEMIC Division of Department of Electrical Engineering (ESAT), KU Leuven, 3001, Leuven, Belgium (e-mail: xiue.bao@esat.kuleuven.be).

I. Ocket is with the Interuniversity Microelectronics Center (IMEC), 3001 Heverlee, Belgium, and also with the ESAT-TELEMIC Division, KU Leuven, 3001 Leuven, Belgium (e-mail: ocket@imec.be).

D. Kil and R. Puers are with the ESAT-MICAS Division, KU Leuven, 3001 Leuven, Belgium (e-mail: robert.puers@kuleuven.be).

Z. Liu is with the Department of Materials Engineering, KU Leuven, 3001 Leuven, Belgium (e-mail: zhuangzhuang.liu@kuleuven.be).

Color versions of one or more of the figures in this paper are available online at http://ieeexplore.ieee.org.

Digital Object Identifier .....

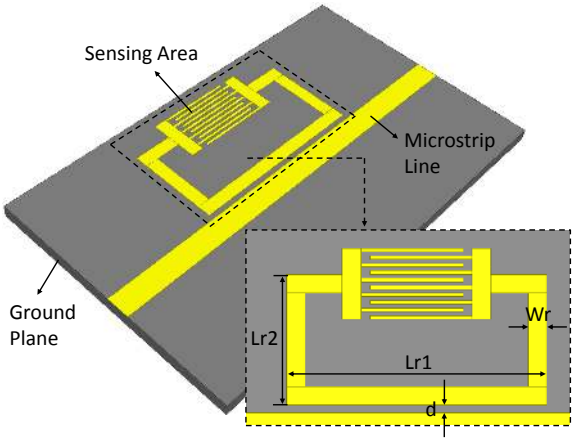

Fig. 1. Topology of the microstrip line excited interdigitated electrodes based split-ring-resonator for biosensing.

is implemented in microstrip transmission line. Extended from previous microstrip line based interdigital capacitor sensor [17], the proposed IDE-SRR sensor combines the advantage of SRR's high sensitivity and IDE's accurate modeling for the linear relationship between its equivalent capacitance and the permittivity of the liquid under test.

The paper is organized as follows. Section II describes the structure of the proposed microstrip IDE-SRR sensor, the fabrication technology, and its sensing concept. In Section III, some existing mixing rules and formulas on the effective permittivity of mixtures are presented. The measurement setup and calibration procedure are explained in Section IV. After a validation measurement, the platform is used to measure two binary mixtures, and the results are reported and discussed. This section also analyzes the existing mixing formulas for calculating the effective permittivity of binary liquid mixtures. Finally, the main conclusions of the work are highlighted in Section V.

II. Architecture, Fabrication, and Theoretical Study of the Proposed Sensor

A. Microstrip Transmission Line Excited SRR Sensor

Fig. 1 depicts the topology of the proposed microstrip transmission line excited IDE-SRR sensor. The sensor is designed on a $1\,\mathrm{mm}$ thick Borofloat 33 glass wafer, of which the real part of the dielectric permittivity (ε_r) and loss tangent ($tan\delta$) are 4.6 and 0.0037 (at 1 MHz and 25°C), respectively. Due to the stable electrical properties within a broad bandwidth, its perfect transparency, and ease of dicing, Borofloat 33 glass is herein used as the substrate. The coplanar split ring is designed on one side of the microstrip line, located at close proximity to the microstrip line for effective excitation by the time-varying magnetic field of the line. Here, the microstrip line behaves as an open conduit for wave propagation so that the electromagnetic fields are not entirely confined under the signal line. The field components on the ring excite the resonator, with strong and high sensitivity resonance being created. Different from generally seen SRR, several interdigitated electrodes are etched on the ring as the split gap, forming the sensing area of the proposed sensor. The interdigitated electrodes are aimed at generating a large capacitance, considerably lowering the resonance frequency and concentrating the electric field. Theoretical analysis of the interdigitated electrodes has been previously presented in detail [30].

As shown in Fig. 1, the distance between the ring and the microstrip line is denoted by d; the length along the strip line, the length perpendicular to the strip line, and the width of the ring are denoted as L_{r1}, L_{r2}, and W_r, respectively. The finger width w_f, length l_f, gap between fingers s_f, the space by the end of each finger g_f, and the total number of fingers n_f at the IDE sensing area are designed at $0.2\,\mathrm{mm}$, $5.5\,\mathrm{mm}$, $0.2\,\mathrm{mm}$, $0.5\,\mathrm{mm}$, and 10, respectively. The microstrip line has a width of $1.8\,\mathrm{mm}$ and a length of $32\,\mathrm{mm}$, corresponding to a characteristic impedance of approximately 50 Ω.

B. Sensor Fabrication

The IDE-SRR sensor was fabricated by using standard photolithography and chemical etching techniques [31]. The IDE-SRR sensing layer was patterned on the surface of the Borofloat 33 glass wafer with a typical lift-off technology. First, the glass wafer was cleaned in a boiling Piranha solution (H2SO4:H2O2 = 3:1) for 10 minutes, which was followed by a dehydration process under 200°C for 2 minutes. Second, $1\,\mu\mathrm{m}$ thick LOR 10B followed by $1\,\mu\mathrm{m}$ thick S1818 photoresist was spin-coated on the wafer. Third, after soft baking, the two photoresist layers were exposed to UV light through a pattern mask, and then they were developed in the corresponding photoresist developer (351 Dev:H2O=1:4) to remove the exposed parts. Next, through sputtering deposition technique, the wafer was coated with a Titanium (Ti) adhesion layer at a thickness of $\sim 50\,\mathrm{nm}$, followed by top-coating with a gold (Au) layer at a thickness of $\sim 400\,\mathrm{nm}$. The final lift-off process for pattering the sensing electrodes was completed by immersing the glass wafer in N-Methylpyrrolidone (NMP) for two days to remove the rest LOR 10B and S1818 photoresist together with the unwanted metal parts.

The ground layer of the microstrip IDE-SRR sensor was fabricated by bounding the bottom of the glass substrate with a piece of $35\,\mu\mathrm{m}$ thick conductive electrodeposited copper foil. Next, the two ports of the microstrip IDE-SRR sensor were connected to two SMA connectors, using silver conductive paint (SCP) and solder for the gold signal layer and the copper ground layer, respectively.

For liquid confinement, a rectangular Polydimethylsiloxane (PDMS) ring was bounded to the surface of the microstrip IDE-SRR sensor, assuring that the liquid under test (LUT) can be loaded on top of the sensing area. The thickness of the PDMS ring was designed at $3\,\mathrm{mm}$ to guarantee that the permittivity measurement of the liquid mixtures is independent of the LUT thickness [30]. The Borofloat glass has excellent hydrolytic resistance, acid resistance, and alkali resistance. Additionally, it has a mirror like surface and high thermal resistance. Therefore, the surface of the Borofloat 33 glass wafer at the sensing area was not specifically processed for the liquid measurements.

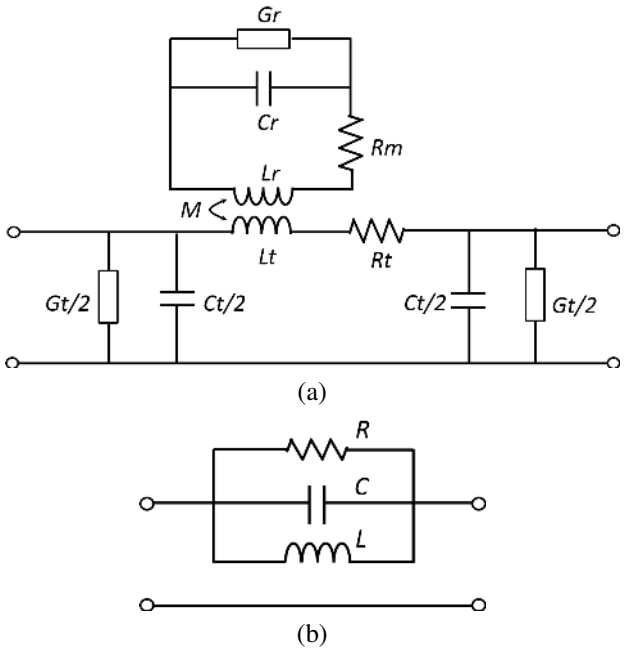

Fig. 2. Equivalent circuit of the microstrip line excited IDE-SRR sensor (a) and its simplified equivalent circuit at the resonance frequency [32] (b).

C. Equivalent Circuit and Detecting Theory

Due to the small electrical dimensions of the sensor compared to the wavelengths of the frequency range considered, the IDE-SRR structure can be described by means of a lumped element equivalent circuits. As shown in Fig. 2(a), the microstrip transmission line is typically modeled with a series inductance L_t, a series resistance R_t, a parallel capacitance C_t, and a parallel conductance G_t. The equivalent inductance due to the IDE-SRR loop is represented with L_r, while R_m is caused by the metal of the IDE-SRR loop. In Fig. 2(a), the equivalent capacitance C_r and the parallel conductance G_r are mainly dependent on the LUT permittivity properties [9]. Effectively, the IDE-SRR can be equivalent to a series RLC resonant circuit, with the resonance frequency and Q factor being obtained by

$$\omega_{res} = 2\pi f_{res} = \frac{1}{\sqrt{L_r C_r}} \tag{1}$$

$$Q_r = \frac{1}{R_r}\sqrt{\frac{L_r}{C_r}} \tag{2}$$

where the equivalent resistance R_r is a combination of the effects of G_r and R_m.

The IDE-SRR structure is magnetically coupled to the microstrip line through a mutual inductance, M, which is approximated by $M = L_r \cdot \alpha F$, where F is the fraction of the cell area occupied by the IDE-SRR and α is a fitting parameter. Near the resonance frequency f_{res}, the IDE-SRR loaded transmission line can be modeled as a simplified equivalent circuit as shown in Fig. 2(b) [33], [34], where $L = M^2/L_r$, $C = C_r L_r^2/M^2$, $R = M^2/(C_r L_r R_r)$, and $\omega_{res}^2 = 1/(LC) = 1/(L_r C_r)$ $Q_r = R\sqrt{C/L} = R_r^{-1}\sqrt{L_r/C_r}$

From our previous research [28], [30], the equivalent capacitance of an IDE structure has the following linear relationship with the real permittivity of the material loaded on top of the IDE sensing area

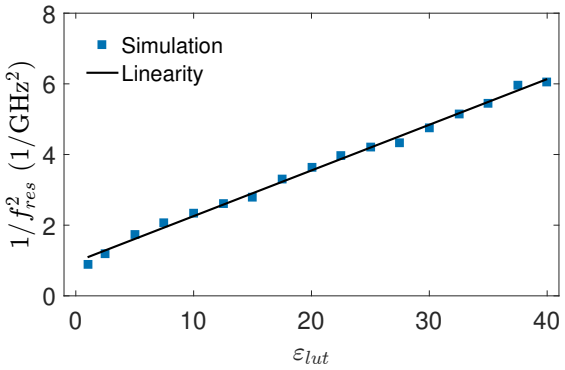

Fig. 3. Simulation validation of the linear correlation between $1/f_{res}^2$ and the relative real part permittivity ε_{lut} of the liquid on top of the IDE-SRR sensing area.

$$C_{IDE} = q_1 + q_2 \cdot \varepsilon_{sub} + q_3 \cdot \varepsilon_{lut} \tag{3}$$

where ε_{sub} and ε_{lut} denote the permittivity of the substrate and the LUT, respectively, and q_1, q_2, and q_3 are determined by the dimensions of the IDE structure. Therefore, C_r in Fig. 2(a) can be roughly approximated by $C_r = C_0 + q \cdot \varepsilon_{lut}$, where C_0 represents the capacitance of the empty device at the IDE-SRR ring, including the capacitive effect of the dielectric substrate and the PDMS container, whereas the term $q \cdot \varepsilon_{lut}$ describes the contribution of the loaded liquid. ε_{lut} is the real part permittivity of the LUT and q presents the linear relationship between ε_{lut} and C_r [9].

Consequently, according to (1), it is reasonable to assume that $1/f_{res}^2$ is linearly dependent on the LUT's real part permittivity ε_{lut}. To validate the linearity, a series of three dimensional (3D) simulations were performed on the sensing area of the IDE-SRR structure with a finite element method (FEM). A given LUT is assumed to be loaded on top of the IDE-SRR sensing area. With the LUT imaginary part permittivity being constant, the real part permittivity ε_{lut} is set at 1, 2.5, 5, 7.5, ..., 40 consecutively. After each simulation, the resonance frequency f_{res} is determined, and subsequently $1/f_{res}^2$ is calculated. Fig. 3 depicts the simulation results, which reveals a good linear correlation of $1/f_{res}^2$ and ε_{lut}. Some researches show that liquids can be detected with the Q factor of a resonator or the transmission coefficient [25], but to our experience, it is mainly used for a small variation of the imaginary permittivity of a material under observation. Therefore, the IDE-SRR is herein designed to detect the LUT's real part of the permittivity.

The resonance frequency is also highly correlated with the dimensions of the IDE-SRR structure. To discover the correlation, we performed a series of full-wave 3D FEM simulations on the bare IDE-SRR sensor. Fig. 4(a), (b), (c), and (d) presents the correlation of IDE-SRR resonance frequency f_{res} with the dimensions L_{r1}, L_{r2}, W_r, and d, respectively. Obviously, with longer L_{r1} or L_{r2}, smaller f_{res} is obtained, whereas larger W_r leads to larger f_{res}. This phenomenon validates (1), as longer L_{r1} or L_{r2} leads to

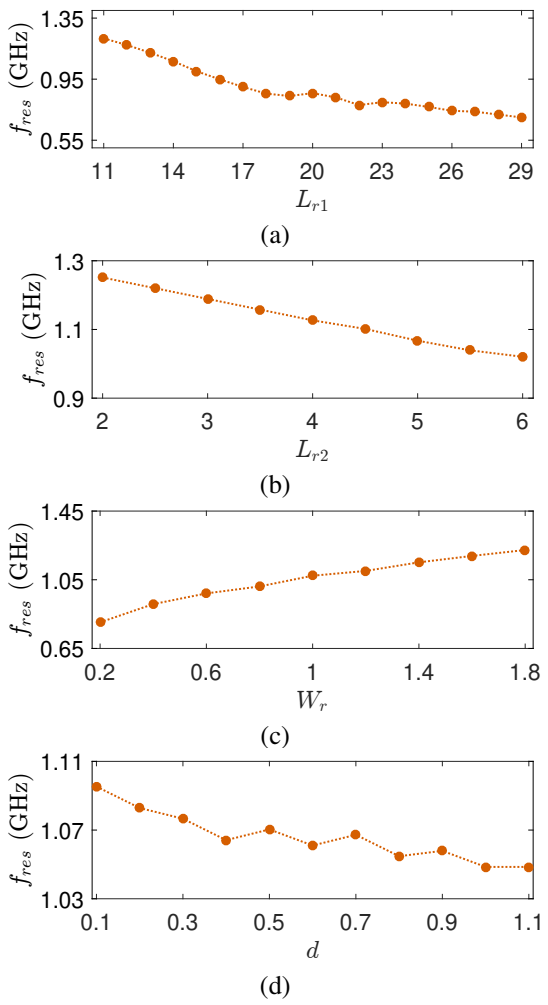

Fig. 4. Effects of the dimensions (a) L_{r1}, (b) L_{r2}, (c) W_r, and (d) d on the resonance frequency f_{res} values based on full-wave 3D FEM simulations.

the increase of L_r, resulting in smaller resonance frequency f_{res}. In contrast, if we increase W_r, the equivalent inductance L_r is decreased, resulting in larger f_{res}. Though there is a little fluctuation in Fig. 4(d), which is mainly related to the accuracy limitation of the finite element simulation method, the approximate conclusion that larger d leads to relative smaller f_{res} could be reached. The above conclusions can work as the optimization principles of the IDE-SRR sensor design. Considering the device optimization and the fabrication resolution, for the IDE-SRR sensor herein used, L_{r1}, L_{r2}, W_r, and d are correspondingly designed at $14\,\mathrm{mm}$, $7\,\mathrm{mm}$, $1\,\mathrm{mm}$, and $0.4\,\mathrm{mm}$. At the sensing area, there are 10 interdigitated electrodes. The electrode length, the electrode width, the space between electrodes, the space by the end of each electrode are $5.5\,\mathrm{mm}$, $0.2\,\mathrm{mm}$, $0.2\,\mathrm{mm}$, and $0.5\,\mathrm{mm}$, respectively. Therefore, the liquid volume at the sensing area is around $0.068\,\mathrm{mL}$ ($6{\times}3.8{\times}3\,\mathrm{mm}^3$).

III. Mixing Models of Binary Mixtures

In electromagnetism, when the ratio between the size of the inhomogeneities and the wavelength of the electromagnetic field is much smaller than unity, the medium acts as a homogeneous dielectric layer to the wave with an effective permittivity. If correct homogenisation is used, one can accurately relate the effective dielectric values to the amount of components in the media. The internal properties of heterogeneous media being sought using a measured macroscopic observable, is actually the inversion of the mixing rule, which predicts the effective permittivity of a mixture as a function of its components. The homogenisation requires a quasistatic nature of the media, which means that the diameter of the molecules that can be recognized are small compared to the wavelengths of the electromagnetic field.

The binary mixture herein is assumed to consist of two dielectric components, of which one is treated as host and the other as the inclusion phase. In the literature, many mixing models can be found for the effective dielectric permittivity of such a mixture. However, no model seems to be able to predict the dielectric behavior over the whole range of volume fraction of a mixture [35]. Here we present some typical ones. For the case of circular inclusions, the effective permittivity of a mixture can be predicted according to the classic Maxwell Garnett (MG) mixing rule [14]

$$\varepsilon_m = \varepsilon_1 \frac{(2\varepsilon_1+\varepsilon_2)+2v_2(\varepsilon_2-\varepsilon_1)}{(2\varepsilon_1+\varepsilon_2)+v_2(\varepsilon_2-\varepsilon_1)} \tag{4}$$

where circular inclusions of permittivity ε_1 are randomly distributed in a homogeneous environment of permittivity ε_2 with a volume of the scatterer v_2 and occupy a volume fraction of v_1. Together with the MG theory, the oldest and most popular mixing rule is the following Bruggeman formula [13]

$$v_1\frac{\varepsilon_1-\varepsilon_m}{\varepsilon_1+\varepsilon_m}+v_2\frac{\varepsilon_2-\varepsilon_m}{\varepsilon_2+\varepsilon_m}=0 \tag{5}$$

In some modelling analyses, the following power-law model is proposed

$$\varepsilon_m^\alpha = v_1\varepsilon_1^\alpha + v_2\varepsilon_2^\alpha, -1\le\alpha\le 1 \tag{6}$$

which leads to the Birchak formula [36] and Looyenga formula [37] with α being 1/2 and 1/3, respectively; and for the case $\alpha\to 0$, (6) turns out to be the following Lichtenecker formula [35], [38]

$$ln\varepsilon = v_1 ln\varepsilon_1 + v_2 ln\varepsilon_2 \tag{7}$$

Besides, the Bottcher formula, in the expression of

$$\varepsilon_m = \varepsilon_1 + \frac{3v_2\varepsilon_m(\varepsilon_2-\varepsilon_1)}{2\varepsilon_m+\varepsilon_2} \tag{8}$$

the Raleighs formula, expressed as

$$\varepsilon_m = \varepsilon_1 \frac{\frac{2\varepsilon_1+\varepsilon_2}{\varepsilon_2-\varepsilon_1}+2v_2-\frac{1.57(\varepsilon_2-\varepsilon_1)}{4\varepsilon_1+3\varepsilon_2}v_2^{3.33}}{\frac{2\varepsilon_1+\varepsilon_2}{\varepsilon_2-\varepsilon_1}-v_2-\frac{1.57(\varepsilon_2-\varepsilon_1)}{4\varepsilon_1+3\varepsilon_2}v_2^{3.33}} \tag{9}$$

and the Meredith and Tobias formula in the form of

$$\varepsilon_m = \varepsilon_1 \frac{\frac{2\varepsilon_1+\varepsilon_2}{\varepsilon_2-\varepsilon_1}+2v_2-1.277\frac{2\varepsilon_1+\varepsilon_2}{4\varepsilon_1+3\varepsilon_2}v_2^{7/3}-6.399\frac{\varepsilon_2-\varepsilon_1}{4\varepsilon_1+3\varepsilon_2}v_2^{10/3}}{\frac{2\varepsilon_1+\varepsilon_2}{\varepsilon_2-\varepsilon_1}-v_2-1.277\frac{2\varepsilon_1+\varepsilon_2}{4\varepsilon_1+3\varepsilon_2}v_2^{7/3}-2.718\frac{\varepsilon_2-\varepsilon_1}{4\varepsilon_1+3\varepsilon_2}v_2^{10/3}} \tag{10}$$

are also often used to analyze liquid mixtures.

By analyzing laminar mixtures, Wiener proposed the following formula [39]

$$\frac{\varepsilon_m-\varepsilon_2}{\varepsilon_m+u\varepsilon_2}=v_1\frac{\varepsilon_1-\varepsilon_2}{\varepsilon_1+u\varepsilon_2}, 0\le u\le\infty \tag{11}$$

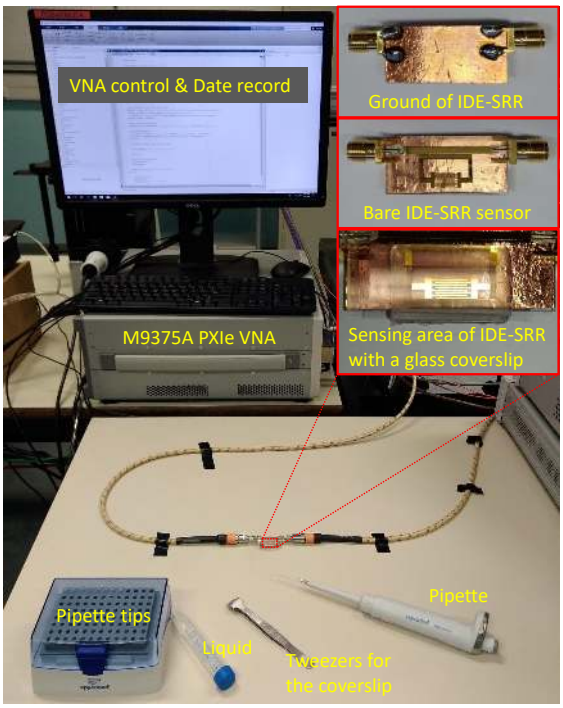

Fig. 5. The IDE-SRR sensor and the measurement setup used for measuring the effective permittivity of binary mixtures.

where for isotropic materials, Bruggman suggested $u = \sqrt{\varepsilon_1 \varepsilon_2}$. When u is 2, the formula is equivalent to Maxwell-Garnett equation which has been used to analyze nanofluids [40]. If u is set at 0 and ∞, respectively, (11) defines the effective permittivity bounds (i.e., Wiener (W) bounds), as

$$\varepsilon_{m,max} = v_1 \varepsilon_1 + v_2 \varepsilon_2 \tag{12a}$$

$$\varepsilon_{m,min} = \frac{\varepsilon_1 \varepsilon_2}{v_1 \varepsilon_2 + v_2 \varepsilon_1} \tag{12b}$$

Hashin-Shtrikman (HS) bounds are also generally accepted to analyze statistically homogeneous and isotropic mixtures [41]. The HS bounds are expressed as

$$\varepsilon_{m,max} = \varepsilon_1 + \frac{v_2}{1/(\varepsilon_2 - \varepsilon_1) + v_1/(2\varepsilon_1)} \tag{13a}$$

$$\varepsilon_{m,min} = \varepsilon_2 + \frac{v_1}{1/(\varepsilon_1 - \varepsilon_2) + v_2/(2\varepsilon_2)} \tag{13b}$$

where it is assumed that $\varepsilon_1 > \varepsilon_2$.

IV. Measurements and Discussion

A. Measurement Setup and Calibration

The liquid measurements were carried out with a Keysight M9375A PXIe Vector Network Analyzer (VNA), as shown in Fig. 5. Its two ports were separately connected to the two SMA connectors of the IDE-SRR sensor. Before doing any measurements, a two-port short-open-load-thru (SOLT) calibration routine was conducted to remove the errors caused by the cables and connections between the VNA and the SMA connectors. This process was accomplished with a commercial Agilent 85052B 3.5 mm calibration kit and its associated parameters as provided by the vendor. During the calibration process and also for the subsequent liquid measurements, the VNA frequency was swept from 300 kHz to 3 GHz and the VNA power was set at -20 dBm to reduce the unwanted potential microwave heating effect. Each liquid measurement was performed within 1 minute. To our experience, the potential heating effect at -20 dBm for 0.068 mL within less than 1 minute measurement can be neglected [42]. During the liquid measurements, an air conditioning system was used to keep the room temperature at around 20°C and a piece of glass coverslip was placed on top of the PDMS liquid container (as presented in Fig. 5). Therefore, for the liquid volume used herein, the measurement effect caused by any potential liquid evaporation can be ignored. After each measurement, the IDE-SRR device was cleaned with deionized water and carefully blow-dried.

B. Validation with Water-Isopropanol Mixtures

A binary mixture of deionized water and isopropanol (percent purity 99.9%) of different fractions is chosen to validate the detecting theory proposed in previous section. The volume fraction ($v/v\%$) of isopropanol varies from 0% to 100% with a step size of 5%, leading to a dataset of 21 groups of water-isopropanol solutions. The 21 groups of water-isopropanol mixtures are first measured with the proposed IDE-SRR sensor. For each liquid mixture, measurements were performed five times, with the measurement repeatability error within approximately 2.5%. The resonance frequency of the empty IDE-SRR sensor is at 1.058 GHz and the calculated Q factor with the 3 dB bandwidth method [43] is 12.5. When the sensor was filled with water-isopropanol mixtures, as the volume fraction of isopropanol varied from 0% to 100%, the resonance frequency increased from 447.84 MHz to 897.60 MHz. As reference, the pure deionized water (0%), the pure isopropanol (100%), and the 19 groups of mixtures were also measured with a microstrip line exited interdigital capacitor sensor [17], from which we can directly obtain the real part of the permittivity of each measured liquid mixture. The measured resonance frequencies obtained with the IDE-SRR method were combined with the permittivity obtained with the interdigital capacitor sensor (at the randomly chosen frequency of 500 MHz), leading to the plot in Fig. 6.

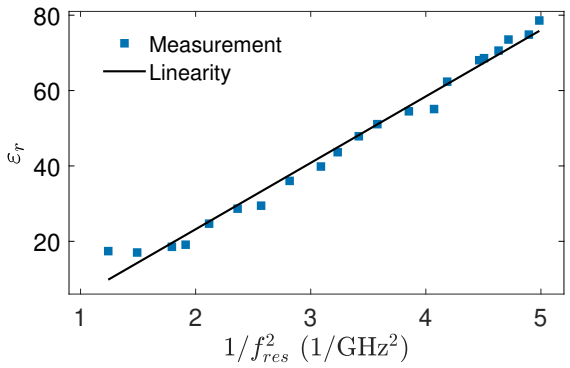

Fig. 6. Validation of the detecting theory via the measurement results of water-isopropanol mixtures, with $R^2 = 0.9843$.

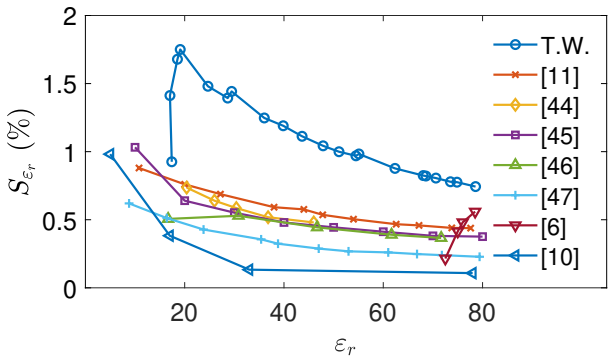

Fig. 7. Sensitivity comparison of the proposed sensor with state-of-the-art devices corresponding to real part of the permittivity of the tested samples.

Fig. 6 shows the IDE-SRR measurement results with the liquid real part permittivity ε_r as a function of the resonance frequency f_{res} as follows

$$\varepsilon_r = 17.625 \times 1/f_{res}^2 - 12.052 \tag{14}$$

where ε_r was extracted from the measurement results of the 21 water-isopropanol mixtures using the microstrip interdigital capacitor technique and f_{res} was calculated from the proposed IDE-SRR sensor. As can be seen from Fig. 6, formula (14) reveals a good linear correlation (fitting $R^2 = 0.9843$) between ε_r and $1/f_{res}^2$.

TABLE I
COMPARISON OF STATE-OF-ART MICROWAVE MICROFLUIDIC SENSORS

Ref.	Sens. Method	Sample Volume (μL)	f_{empty} (GHz)	Meas. Error of ε_r
[11]	LCR	0.39	1.91	3.90%
[44]	CPW Resonator	3.6×10^{-7}	22.62	6.40%
[45]	SRR	5	2.6	6.4%
[46]	LCR	N/A	2.05	N/A
[47]	CSRR	0.588	2.02	8.50%
[6]	CSRR	100	4.65	N/A
[10]	SRR	N/A	5.78	N/A
T.W.	IDE-SRR	68	1.06	2.5%

Fig. 7 presents the sensitivity of the IDE-SRR, with the sensitivity definition [11] as

$$S_{\varepsilon_r} = \frac{f_{\varepsilon_r} - f_{empty}}{f_{empty} \cdot (\varepsilon_r - 1)} \times 100 \tag{15}$$

where f_{ε_r} is the resonance frequency of the proposed IDE-SRR sensor, which is loaded with LUT whose real part permittivity is ε_r; and f_{empty} is the resonance frequency of the empty sensor. Sensitivity of the proposed sensor is calculated from the measurement results of water-isopropanol mixtures. The sensitivity of some other state-of-the-art resonance based microwave microfluidic sensors [6], [10], [11], [44]–[47] are also presented in Fig. 7. The future trend of dielectric sensors is high sensitivity over broad range of permittivity values, simple integration with other electronics, and small sample volume. Considering the advantages of simple manufacturing procedures and better compatibility with other electronics, the sensors used for comparison here are all planar structures. A general conclusion can be drawn that the designed IDE-SRR sensor excels in sensitivity for real permittivity measurements, behaving quite better than the other devices. For the IDE-SRR sensitivity, a drop at permittivity value around 20 can be seen in Fig. 7. This is caused by a measurement error of the reference permittivity obtained with the interdigital capacitor sensor [17].

Other important factors are analyzed for comparison as well and presented in Table I. The sensors of [11] and [46] have simple structures of LC resonator, and other sensors used for comparison here are based on the SRR structure but with different configurations. [45] introduces a metamaterial transmission line feeding SRR to increase sensitivity and [10] used 3D printing to make wide range permittivity detection sensor with a tunable gap between feeding TL and SRR. [47] uses complementary SRR at resonant frequency to perform detection, while [6] designed a fluidic channel which covers the entire gap of a complementary SRR to have a deep null for sensitivity. For most of the considered sensors, large permittivity measurement range can be achieved, except [44] that works at K-band to achieve a small sample volume. Compared to other devices, the IDE-SRR sensor proposed in this work, operates at low RF/microwave frequencies and has high measurement accuracy. The sample volume of the proposed sensor is large, but it can be readily reduced with a high resolution fabrication technique, while its high sensitivity and low ε_r measurement error have proved its novelty.

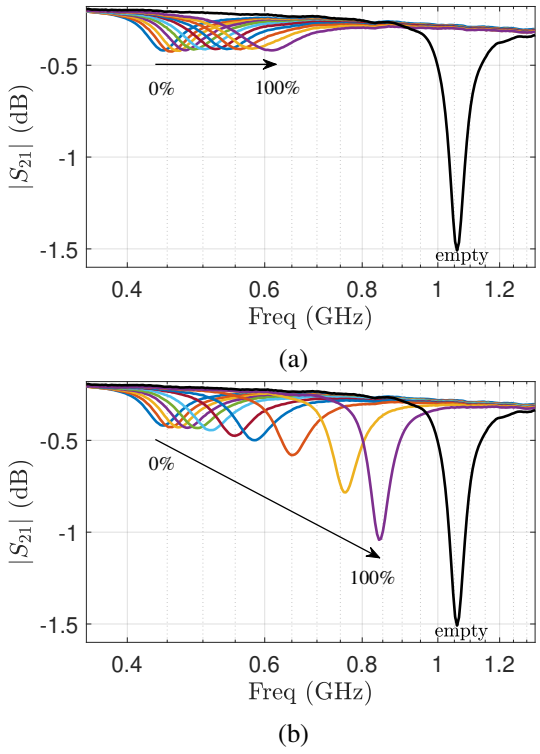

Fig. 8. Measured insertion loss of (a) water-MeOH mixtures loaded IDE-SRR sensor and (b) water-THF mixtures loaded IDE-SRR sensor, with the empty sensor as a reference.

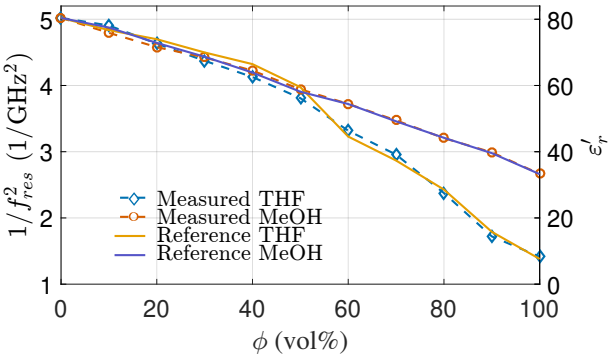

Fig. 9. Correlation of the measured $1/f_{res}^2$ with the infraction of THF and MeOH for the water-THF and water-MeOH mixtures, respectively. As a reference, the real part permittivity at each infraction of the two types of mixtures are also shown.

C. Measurement Results and Analysis of Two Binary Mixtures

After the validation measurement, the IDE-SRR sensor was loaded with a series of water-methanol (MeOH) mixtures having MeOH fraction in a range of 0% to 100% with step of 10% and a series of water-tetrahydrofuran (THF) mixtures having THF volume fraction in a range of 0% to 100% with step of 10%. When the IDE-SRR sensor is loaded with water-MeOH mixtures of different concentrations, the measured transmission response of the sensor is given in Fig. 8(a). To make the plot more readable, the horizontal axis is presented in the logarithmic form. The resonance frequency is lowered from 0.613 GHz to 0.446 GHz, as the water concentration increases from 0% to 100%. Similarly, the measured transmission responses of the IDE-SRR sensor loaded with the different water-THF mixtures are presented in Fig. 8(b). As the THF fraction increases from 0% to 100%, the resonance frequency increases from 0.446 GHz to 0.841 GHz. In Fig. 8(a) and (b), the empty IDE-SRR sensor works as a reference, with the resonance frequency at approximately 1 GHz. Apparently, the absolute S_{21} resonance values of water-THF mixtures decreases from -0.5 to -1 with THF fraction increasing from 0% to 100%, whereas the values for water-methanol mixtures approximately stay constant. The difference is correlated with the imaginary part of the permittivity of the liquid mixtures, which is rather complex and beyond the topic discussed here.

Based on the measurement results in Fig. 8(a) and (b), $1/f_{res}^2$ values of the two types of mixtures at each concentration are calculated and presented in Fig. 9. As reference, the extracted real part permittivity values measured with the microstrip interdigital capacitor technique [17] are also shown in Fig. 9. Clearly, perfect agreements between the $1/f_{res}^2$ obtained with the proposed IDE-SRR method and the ε_r obtained with the microstrip interdigital capacitor device are observed for both types of mixtures.

Using the previously obtained equation (14), we are able to extract the real part permittivity values of the water-THF mixtures and the water-MeOH mixtures at each concentration. The extracted results are presented in Fig. 10 and Fig. 11, respectively. The corresponding literature data of water-MeOH [48] mixtures and water-THF [49] are also plotted in Fig. 10 and Fig. 11, respectively. Obviously, the permittivity values of both water-MeOH mixtures and water-THF mixtures measured with the proposed IDE-SRR technique show very good agreement with literature data [48], [49]. Through the comparison, IDE-SRR sensor has further shown the capability of detecting large permittivity variation range with high sensitivity/accuracy compared to a microstrip IDE sensor.

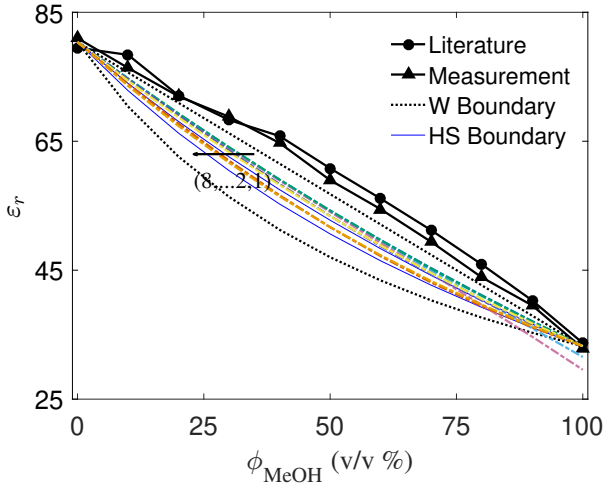

Fig. 10. Correlation of the water-MeOH mixture concentration with the corresponding extracted real part permittivity at 3 MHz, where the number 1 to 8 in turn indicate the calculation results with the Maxwell Garnett mixing rule, the Raleighs formula, the Meredith and Tobias formula, the Birchak formula, the Bottcher formula, the Looyenga's formula, the Bruggeman formula, and the Lichtenecker formula. The literature data measured with previous method are also added as a comparison [17].

Next, using the measured ε_r of water-MeOH solutions at the concentrations of 0% and 100%, we are able to calculate the permittivity of each mixture at any other concentration

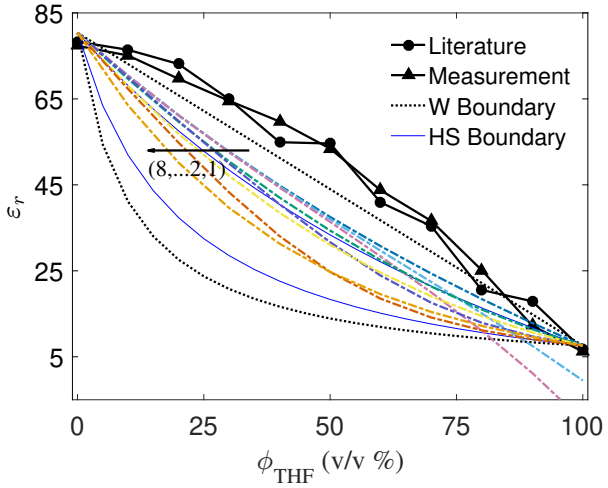

Fig. 11. Correlation of the water-THF mixture concentration with the corresponding extracted real part permittivity at 3 MHz, where the number 1 to 8 in turn indicates the calculation results with the Maxwell Garnett mixing rule, the Raleighs formula, the Meredith and Tobias formula, the Birchak formula, the Bottcher formula, the Looyenga's formula, the Bruggeman formula, and the Lichtenecker formula. The literature data measured with previous method are also added as a comparison [17].

between 0% and 100% with the given formulas (4) to (11) presented in Section III. Similarly, using the measured ε_r of water-THF solutions at the concentrations of 0% and 100%, we are able to obtain the calculated permittivity of other water-THF mixtures with the concentrations from 10% to 90%. Using equations (12) and (13), we are also able to obtain the effective permittivity boundaries for both water-MeOH mixtures and water-THF mixtures. The calculation results are presented in respectively Fig. 10 and Fig. 11 as well.

Generally, different formulas provide obviously different permittivity results for the same mixture. The difference between the formulas is the most significant when there is half volume of water in the binary mixtures. In both Fig. 10 and Fig. 11, the W-bounds equations provide a large permittivity calculation range, which almost includes all of the effective permittivity results calculated with other formulas. In the W-bounds formulas, (12a) is actually linearly dependent on v_1, as $v_1 + v_2 = 1$. Interestingly, the calculated effective permittivity results obtained with the existing mixing formulas are all beneath the W-bounds linear line, whereas both measurement and literature permittivity data are above the linear Wiener maximum line. Among the eight models, Maxwell Garnett mixing rule comes nearest to the measurement results. The results might indicate that the existing EMA models used to analyze liquid mixtures at zero frequency are not applicable for RF/microwaves frequencies. To estimate the effective permittivity of dielectric materials at high frequencies, a different reliable EMA mixing formula should be developed. It might be helpful to develop the model starting from the Maxwell Garnett mixing rule.

V. Conclusion

Aiming at studying the mixing rules of a binary liquid mixture, we proposed a microstrip line based IDE-SRR sensor. Specially, the IDE-SRR sensing area is designed as interdigitated electrodes. By using an equivalent circuit theory and a three-dimensional finite-element-method, we successfully arrive at a detecting equation that relates the resonance frequency of the proposed IDE-SRR sensor with the permittivity property of a liquid under test. The detecting equation is first validated with water-isopropanol mixtures and then used to measure water-methanol mixtures and water-tetrahydrofuran mixtures. The measurement results show good agreement with literature data.

Next, with the obtained real part permittivity values of deionized water, pure methanol, and pure tetrahydrofuran, we calculated the effective permittivity of water-methanol mixtures and water-tetrahydrofuran mixtures with the existing mixing formulas. Obvious disagreement is observed between the measurement results at RF/microwaves and the calculation results for both water-methanol and water-tetrahydrofuran mixtures. The disagreement indicates that the existing mixing formulas should be improved when used to estimate the effective permittivity of mixtures at RF/microwave frequencies.

Acknowledgment

The authors would like to thank M. Bastin from Centre for Surface Chemistry and Catalysis, Department of Molecular and Microbial Systems, KU Leuven for liquids preparation, G. Maenhout and N. Gaethofs from Electrical Engineering, KU Leuven for wafer dicing, Leuven NanoCentre for device fabrication, and KU Leuven Central Electronic Service for technical support.

References

[1] H. P. Schwan, "Electrical properties of tissue and cell suspensions," in *Advances in biological and medical physics*. Elsevier, 1957, vol. 5, pp. 147–209.

[2] A. Babajanyan, J. Kim, S. Kim, K. Lee, and B. Friedman, "Sodium chloride sensing by using a near-field microwave microprobe," *Appl. Phys. Lett.*, vol. 89, no. 18, p. 183504, Oct. 2006.

[3] J. Kim, A. Babajanyan, A. Hovsepyan, K. Lee, and B. Friedman, "Microwave dielectric resonator biosensor for aqueous glucose solution," *Rev. Sci. Instrum.*, vol. 79, no. 8, p. 086107, Aug. 2008.

[4] A. Bababjanyan, H. Melikyan, S. Kim, J. Kim, K. Lee, and B. Friedman, "Real-time noninvasive measurement of glucose concentration using a microwave biosensor," *J. Sens.*, vol. 2010, Dec. 2010.

[5] S. Kim, H. Melikyan, J. Kim *et al.*, "Noninvasive in vitro measurement of pig-blood d-glucose by using a microwave cavity sensor," *Diabetes Res. Clin. Pr.*, vol. 96, no. 3, pp. 379–384, Jun. 2012.

[6] D. Mondal, N. K. Tiwari, and M. J. Akhtar, "Microwave assisted non-invasive microfluidic biosensor for monitoring glucose concentration," in *2018 IEEE Sensors*. New Delhi, India, 28-31 Oct. 2018, pp. 1–4.

[7] S. Mohammadi, A. V. Nadaraja, D. J. Roberts, and M. H. Zarifi, "Real-time and hazard-free water quality monitoring based on microwave planar resonator sensor," *Sens. Actuator A Phys.*, p. 111663, Nov. 2019.

[8] J. C. Booth, N. D. Orloff, J. Mateu, M. Janezic, M. Rinehart, and J. A. Beall, "Quantitative permittivity measurements of nanoliter liquid volumes in microfluidic channels to 40 GHz," *IEEE Trans. Instrum. Meas.*, vol. 59, no. 12, pp. 3279–3288, Dec. 2010.

[9] X. Bao, I. Ocket, J. Bao *et al.*, "Broadband dielectric spectroscopy of cell cultures," *IEEE Trans. Microw. Theory Techn.*, vol. 66, no. 12, pp. 5750–5759, Oct. 2018.

[10] B. D. Wiltshire and M. H. Zarifi, "3-D printing microfluidic channels with embedded planar microwave resonators for rfid and liquid detection," *IEEE Microw. Wirel. Compon. Lett*, vol. 29, no. 1, pp. 65–67, Dec. 2018.

[11] A. Ebrahimi, J. Scott, and K. Ghorbani, "Ultrahigh-sensitivity microwave sensor for microfluidic complex permittivity measurement," *IEEE Trans. Microw. Theory Techn.*, vol. 67, no. 10, pp. 4269–4277, Oct. 2019.

[12] K. Heileman, J. Daoud, and M. Tabrizian, "Dielectric spectroscopy as a viable biosensing tool for cell and tissue characterization and analysis," *Biosens. Bioelectron.*, vol. 49, pp. 348–359, Nov. 2013.

[13] V. D. Bruggeman, "Berechnung verschiedener physikalischer konstanten von heterogenen substanzen. i. dielektrizitätskonstanten und leitfähigkeiten der mischkörper aus isotropen substanzen," *Annalen der physik*, vol. 416, no. 7, pp. 636–664, Oct. 1935.

[14] A. H. Sihvola and J. A. Kong, "Effective permittivity of dielectric mixtures," *IEEE Trans. Geosci. Remote Sens.*, vol. 26, no. 4, pp. 420–429, Jul. 1988.

[15] X. Zeng, D. Bergman, P. Hui, and D. Stroud, "Effective-medium theory for weakly nonlinear composites," *Phys. Rev. B*, vol. 38, no. 15, p. 10970, Nov. 1988.

[16] F. Bordi, C. Cametti, and T. Gili, "Dielectric spectroscopy of erythrocyte cell suspensions. a comparison between looyenga and maxwell–wagner–hanai effective medium theory formulations," *J. Non-Cryst. Solids*, vol. 305, no. 1-3, pp. 278–284, Jul. 2002.

[17] X. Bao, I. Ocket, M. Zhang, J. Bao, D. Schreurs, and B. Nauwelaers, "Microwave characterization of liquid mixtures with a miniaturized interdigital sensor," in *2019 IEEE MTT-S Int. Microwave Workshop Series on Advanced Materials and Processes for RF and THz Applications (IMWS-AMP)*. Bochum, Germany, 16-18 Jul. 2019, pp. 1–3.

[18] A. Ebrahimi, W. Withayachumnankul, S. Al-Sarawi, and D. Abbott, "High-sensitivity metamaterial-inspired sensor for microfluidic dielectric characterization," *IEEE Sens. J*, vol. 14, no. 5, pp. 1345–1351, Dec. 2014.
[19] N. Sharafadinzadeh, M. Abdolrazzaghi, and M. Daneshmand, "Investigation on planar microwave sensors with enhanced sensitivity from microfluidic integration," *Sens. Actuator A Phys.*, p. 111752, Jan. 2020.
[20] ——, "Highly sensitive microwave split ring resonator sensor using gap extension for glucose sensing," in *2017 IEEE MTT-S Int. Microwave Workshop Series on Advanced Materials and Processes for RF and THz Applications (IMWS-AMP)*. Pavia, Italy, 20-22 Sep. 2017, pp. 1–3.
[21] P. Velez, K. Grenier, J. Mata-Contreras, D. Dubuc, and F. Martín, "Highly-sensitive microwave sensors based on open complementary split ring resonators (OCSRRs) for dielectric characterization and solute concentration measurement in liquids," *IEEE Access*, vol. 6, pp. 48 324–48 338, Sep. 2018.
[22] A. K. Horestani, J. Naqui, Z. Shaterian, D. Abbott, C. Fumeaux, and F. Martín, "Two-dimensional alignment and displacement sensor based on movable broadside-coupled split ring resonators," *Sens. Actuator A Phys.*, vol. 210, pp. 18–24, Apr. 2014.
[23] H.-J. Lee and J.-G. Yook, "Biosensing using split-ring resonators at microwave regime," *Appl. Phys. Lett.*, vol. 92, no. 25, p. 254103, May 2008.
[24] H.-J. Lee, H.-S. Lee, K.-H. Yoo, and J.-G. Yook, "DNA sensing based on single element planar double split-ring resonator," in *2009 IEEE MTT-S Int. Microwave Symp. Dig.*, 2009, pp. 1685–1688.
[25] P. Vélez, L. Su, K. Grenier, J. Mata-Contreras, D. Dubuc, and F. Martín, "Microwave microfluidic sensor based on a microstrip splitter/combiner configuration and split ring resonators (SRRs) for dielectric characterization of liquids," *IEEE Sens. J*, vol. 17, no. 20, pp. 6589–6598, Oct. 2017.
[26] P. Vélez, J. Mata-Contreras, D. Dubuc, K. Grenier, and F. Martín, "Solute concentration measurements in diluted solutions by means of split ring resonators," in *48th European Microwave Conference (EuMC)*. Madrid, Spain, 23-27 Sep. 2018, pp. 231–234.
[27] P. Vélez, J. Muñoz-Enano, K. Grenier, J. Mata-Contreras, D. Dubuc, and F. Martín, "Split ring resonator-based microwave fluidic sensors for electrolyte concentration measurements," *IEEE Sens. J*, vol. 19, no. 7, pp. 2562–2569, Dec. 2018.
[28] X. Bao, I. Ocket, G. Crupi *et al.*, "A planar one-port microwave microfluidic sensor for microliter liquids characterization," *IEEE J. Electromagn. RF Microw. Med. Biol.*, vol. 2, no. 1, pp. 10–17, Feb. 2018.
[29] D. Lu, Y. Zheng, A. Penirschke, and R. Jakoby, "Highly sensitive dual-mode relative humidity sensor based on integrated SAW and LC resonators," *Electron. Lett*, vol. 51, no. 16, pp. 1219–1220, Aug. 2015.
[30] X. Bao, I. Ocket, J. Bao *et al.*, "Modeling of coplanar interdigital capacitor for microwave microfluidic application," *IEEE Trans. Microw. Theory Techn.*, vol. 67, no. 7, pp. 2674–2683, Jun. 2019.
[31] X. Bao, S. Liu, I. Ocket *et al.*, "A general lineline method for dielectric material characterization using conductors with the same cross-sectional geometry," *IEEE Microw. Wirel. Compon. Lett.*, vol. 28, no. 12, pp. 356–358, Apr. 2018.
[32] A. K. Horestani, C. Fumeaux, S. F. Al-Sarawi, and D. Abbott, "Split ring resonators with tapered strip width for wider bandwidth and enhanced resonance," *IEEE Microw. Wirel. Compon. Lett.*, vol. 22, no. 9, pp. 450–452, Aug. 2012.
[33] J. D. Baena, J. Bonache, F. Martin *et al.*, "Equivalent-circuit models for split-ring resonators and complementary split-ring resonators coupled to planar transmission lines," *IEEE Trans. Microw. Theory Techn.*, vol. 53, no. 4, pp. 1451–1461, Apr. 2005.
[34] X. Q. Lin and T. J. Cui, "Controlling the bandwidth of split ring resonators," *IEEE Microw. Wirel. Compon. Lett.*, vol. 18, no. 4, pp. 245–247, Mar. 2008.
[35] K. K. Karkkainen, A. H. Sihvola, and K. I. Nikoskinen, "Effective permittivity of mixtures: Numerical validation by the FDTD method," *IEEE Trans. Geosci. Remote Sens.*, vol. 38, no. 3, pp. 1303–1308, May 2000.
[36] J. R. Birchak, C. G. Gardner, J. E. Hipp, and J. M. Victor, "High dielectric constant microwave probes for sensing soil moisture," *Proc. IEEE*, vol. 62, no. 1, pp. 93–98, Jul. 1974.
[37] H. Looyenga, "Dielectric constants of heterogeneous mixtures," *Physica*, vol. 31, no. 3, pp. 401–406, Mar. 1965.
[38] K. Lichtenecker, "Die herleitung des logarithmischen mischungsgesetzes aus allgemeinen prinzipien der stationaren stromung," *Phys. Z*, vol. 32, pp. 255–260, Feb. 1931.
[39] S. Evans, "Dielectric properties of ice and snow–a review," *J. Glaciol.*, vol. 5, no. 42, pp. 773–792, Jan. 1965.
[40] J. Miao, M. Dong, M. Ren, X. Wu, L. Shen, and H. Wang, "Effect of nanoparticle polarization on relative permittivity of transformer oil-based nanofluids," *J. Appl. Phys.*, vol. 113, no. 20, p. 204103, May 2013.
[41] Z. Hashin and S. Shtrikman, "A variational approach to the theory of the effective magnetic permeability of multiphase materials," *J. Appl. Phys.*, vol. 33, no. 10, pp. 3125–3131, Jun. 1962.
[42] T. Markovic, J. Bao, G. Maenhout, I. Ocket, and B. Nauwelaers, "An interdigital capacitor for microwave heating at 25 ghz and wideband dielectric sensing of nl volumes in continuous microfluidics," *Sensors*, vol. 19, no. 3, p. 715, Feb. 2019.
[43] D. Rabus, M. Hamacher, U. Troppenz, and H. Heidrich, "High-Q channel-dropping filters using ring resonators with integrated SOAs," *IEEE Photonics Technol. Lett.*, vol. 14, no. 10, pp. 1442–1444, Nov. 2002.
[44] D. D. Thomas Chretiennot and K. Grenier, "A microwave and microfluidic planar resonator for efficient and accurate complex permittivity characterization of aqueous solutions," *IEEE Trans. Microw. Theory Techn.*, vol. 61, no. 2, pp. 972–978, Feb. 2013.
[45] M. D. Mohammad Abdolrazzaghi and A. K. Iyer, "Strongly enhanced sensitivity in planar microwave sensors based on metamaterial coupling," *IEEE Trans. Microw. Theory Techn.*, vol. 66, no. 4, pp. 1843–1855, Jan. 2018.
[46] A. Ebrahimi, J. Scott, and K. Ghorbani, "Microwave microfluidic sensor using microstrip line terminated with LC resonators," in *2019 Int. Conf. Electromagnetics Advanced Applications (ICEAA)*. Granada, Spain, Spain, 9-13 Sep. 2019, pp. 0548–0551.
[47] S. A.-S. Amir Ebrahimi, Withawat Withayachumnankul and D. Abbott, "High-sensitivity metamaterial-inspired sensor for microfluidic dielectric characterization," *IEEE Sens. J*, vol. 14, no. 5, pp. 1345–1351, May. 2014.
[48] S. M. Puranik, A. C. Kumbharkhane, and S. C. Mehrotra, "The static permittivity of binary mixtures using an improved bruggeman model," *J. Mol. Liq.*, vol. 59, no. 2-3, pp. 173–177, Mar. 1994.
[49] A. Kumbharkhane, S. Helambe, M. Lokhande, S. Doraiswamy, and S. Mehrotra, "Structural study of aqueous solutions of tetrahydrofuran and acetone mixtures using dielectric relaxation technique," *Pramana*, vol. 46, no. 2, pp. 91–98, Feb. 1996.

Xiue Bao (S'17) was born in Baoding, China. She received the B.Sc. degree in information engineering in 2011, and the M.Sc. degree in metallurgical engineering in 2013, in the University of Science and Technology Beijing, Beijing, China. She is currently pursuing the Ph.D. degree in electrical engineering at the University of Leuven, Leuven, Belgium. Her current research interests focus on microwave biomedical applications, including broadband dielectric spectroscopy; biosensor design; microwave-microfluidic structure design and fabrication; RF, microwave, and millimeter wave measurement and calibration. She was one of the recipient of the IEEE Microwave Theory and Techniques Society Graduate Fellowship in 2018.

Meng Zhang received the B.S. degree from University of Electronic Science and Technology of China, Chengdu, China, in 2013, and M.S. degree from University of Leuven, Belgium, in 2016, respectively, both in Electrical Engineering. He has been following Postgraduate Program of Biomedical Engineering at University of Leuven, Belgium, since 2017, and currently pursuing the Ph.D degree with a focus on highly sensitive broadband dielectric spectroscopy for biomedical applications at University of Leuven, Belgium.

Ilja Ocket (M'09) received the M.Sc. and Ph.D. degrees in electrical engineering from KU Leuven, Leuven, Belgium, in 1998 and 2009, respectively. He has been with imec, Leuven, and KU Leuven, since 1999. With imec, he is currently involved in millimeter-wave antenna modules and packaging for 79- and 140-GHz radar. With KU Leuven, he leads the group working in the area of microwave and millimeter-wave applications for biology and medicine, and is also involved in integrated couplers for (sub)millimeter plastic waveguides.

Juncheng Bao (S'17) received the M.Sc. degree in electrical engineering from KU Leuven, Leuven, Belgium, in 2013. He had an internship with imec, Leuven, in 2013. He is currently pursuing the Ph.D. degree in electrical engineering at KU Leuven, Leuven, Belgium. His current research interests include microwave biomedical applications, novel microwave-microfluidic devices design and fabrication, microwave and millimeter wave metrology.

Dries Kil received the degree of M.S. of Nanoscience & Nanotechnology from the Katholieke Universiteit Leuven, Belgium, in 2014. The subject of his M.S. thesis was the design and fabrication of a novel neurotrophic electrode based on controlled growth factor release. Since October 2014 he is working as a research assistant at the MICAS group, under the guidance of Prof. Robert Puers, obtaining a Ph.D in Electrical Engineering. His main research is focused on the development of flexible neural probes with a strong focus on biocompatibility and tissue integration.

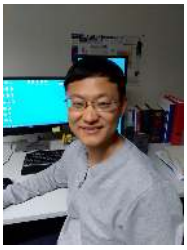

Zhuangzhuang Liu received the master degree in Materials Engineering from Central Iron and Steel Research Institue, Beijing, China, in 2013. He received the Ph.D degree in Materials Engineering from KU Leuven, Leuven, Belgium, in 2017. He is currently a postdoctoral researcher at Department of Materials Engineering, KU Leuven. His current research interests include design of electronic materials and additive manufacturing of multifunctional materials.

Robert Puers (M'86-SM'95-F'11) received the Ph.D. degree from Katholieke Universiteit Leuven (K.U. Leuven), Leuven, Belgium, in 1986. At K.U Leuven, he became Director of the Clean Room Facilities for Silicon and Hybrid Circuit Technology at the ESAT-MICAS laboratories. He was a European pioneer in the research on micromachining, MEMS and packaging techniques, mainly for biomedical implantable systems. To this purpose, he assembled the requested infrastructure, and installed a clean room in 1984, that now runs for more than 25 years under his guidance. Recently, microfluidic and optical MEMS based on polymers are forming the backbone of his sensor research. Beside MEMS, his work focuses also on low power systems, smart interfaces, inductive power and wireless communication. He published design guidelines to improve the efficiency of power induction in two books. He took major efforts to increase the impact of MEMS and microsystems in both the international research community as well as in industry. He helped to launch two spin-off companies.

Dominique Schreurs (S'90-M'97-SM'02-F'12) received the M.Sc. degree in electronic engineering and Ph.D. degree from the University of Leuven, Leuven, Belgium. She is now a Full Professor with KU Leuven and Chair of LICT at KU Leuven. She has been a Visiting Scientist with Agilent Technologies, Santa Rosa, CA, USA; ETH Zurich, Zurich, Switzerland; and the National Institute of Standards and Technology, Boulder, CO, USA. Her current research interests include the microwave and millimeter-wave characterization and modeling of active devices and bioliquids, as well as the system design for wireless communications and biomedical applications.
Prof. Schreurs was an IEEE MTT-S Distinguished Microwave Lecturer and the Editor-in-Chief of the IEEE TRANSACTIONS ON MICROWAVE THEORY AND TECHNIQUES. She was the General Chair of the 2007, 2012, and 2018 ARFTG Conference. She was the Co-Chair of the European Microwave Conference in 2008. She is currently President-Elect of the IEEE MTT-S. She serves as the President of the ARFTG organization.

Bart Nauwelaers (S'80-M'86-SM'99) received the Ph.D. degree in Electrical Engineering from the KU Leuven in 1988. He also received the Master's degree in Design of Telecommunication Systems from Telecom ParisTech, Paris, France. Since 1981, he has been with the Department of Electrical Engineering, KU Leuven, where he has been involved in research on microwave antennas, passive components, interconnects, microwave integrated circuits and MMICs, linear and nonlinear device modeling, MEMS, and wireless communications.
Prof. Nauwelaers is the former chair of IEEE AP/MTT-Benelux and past chair of URSI-Benelux.